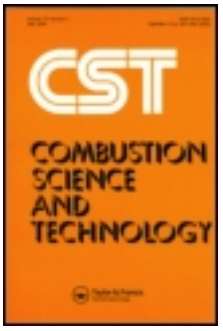

Combustion Science and Technology
Publication details, including instructions for authors and subscription information:
http://www.tandfonline.com/loi/gcst20

Influence of Two-Dimensional Gas Phase Radiation on Downward Flame Spread

TZUNG-HSIEN LIN [a] & CHIUN-HSUN CHEN [a]
[a] Department of Mechanical Engineering , National Chiao Tung University , Hsinchu, Taiwan, 30050, R.O.C
Published online: 27 Apr 2007.

To cite this article: TZUNG-HSIEN LIN & CHIUN-HSUN CHEN (1999) Influence of Two-Dimensional Gas Phase Radiation on Downward Flame Spread, Combustion Science and Technology, 141:1-6, 83-106, DOI: 10.1080/00102209908924183

To link to this article: http://dx.doi.org/10.1080/00102209908924183

Combust. Sci. and Tech., 1999, Vol. 141, pp. 83-106
Reprints available directly from the publisher
Photocopying permitted by license only

Influence of Two-Dimensional Gas Phase Radiation on Downward Flame Spread

TZUNG-HSIEN LIN and CHIUN-HSUN CHEN*

Department of Mechanical Engineering National Chiao Tung University Hsinchu, Taiwan 30050 R.O.C.

(Received May 11, 1998; Revised December 01, 1998)

This work investigates how radiation heat transfer influences downward flame spread by presenting a gas phase radiation model, described by a two dimensional P-1 approximation method, to incorporate with the combustion model of Duh and Chen (1991). The parametric study is based on the variation of gravity, which changes the Damkohler number (Da) and radiation to conduction parameter ($1/N_{\infty}$) simultaneously. Comparing the results with the previous studies of Duh and Chen (1991) and Chen and Cheng (1994), which only considered the radiation effect in cross stream direction, the role of stream-wise radiation was identified. The stream-wise radiation contributes to reinforce the forward heat transfer rate subsequently increasing the flame spread rate. However, this model also provides more directional radiation loss than that of Chen and Cheng (1994) and, in doing so, draws more energy out from the flame to further reduce its strength. The results indicates that the effect of heat loss is greater than that of enhancing the upstream heat transfer since the flame spread rate in the present model is always lower than the one predicted by Duh and Chen (1991). Finally, a contour of the Planck mean absorption coefficient distribution is illustrated to demonstrate the effectiveness of gas radiation distribution. It reveals that the strongest radiation occurs near the pyrolyzing surface and the other significant one is in the plume region. A comparisons with available experimental data also given to evaluate the ability of predict in the present combustion model.

Keywords: downward flame spread; gas phase radiation

INTRODUCTION

This work investigates how radiation influences the downward flame spread behaviors over a thermally thin solid fuel. This work extends the results of our previous study (Chen and Cheng, 1994), which only considered the radiation in cross-stream direction. The stream-wise radiation is naturally added in this

* Correspondence Author.

extended work to complete the combustion model. From this model, we can more thoroughly understand the contribution of stream-wise radiation to the preheating of upstream virgin solid fuel in addition to the forward heat conduction in gas phase by comparing with the results in previous work.

Bhattacharjee et al. (1988) theoretically investigated for the first time how radiative heat transfer influences the flame spread. Those investigators inverted the problem by using the measured surface temperature to obtain the net heat flux from gas to solid. Experimental results were compared with those obtained from theoretical analysis, which neglected all of the radiation effects. Scale analysis indicated that surface radiation may be as important as conduction under a variety of conditions and does not necessarily exist only when the gas-phase velocity is smaller than the flame spread rate. In a related work, Olson et al. (1988) considered the opposed flow diffusion flame spread over a thermally thin cellulose fuel in quiescent and slow forced-flow regimes under microgravity condition. Their results indicated that flame behavior heavily relies on the magnitude of relative velocity between the flame and the atmosphere. That investigation further demonstrated that a high velocity blowoff limit and a low velocity extinction limit exist in a low oxygen concentration environment. Consequently, they developed a flammability boundary consisting of a blowoff and quench branches. Finally, those investigators concluded not only that the flame spread near the quench limit appears to be affected by heat loss from the flame, but also that the use of a Damkohler number alone in the flame spread correlation is inadequate in the low velocity regime. To complete the flame spread date for the entire range of opposed flow velocities and oxygen concentrations, Olson (1991) extended the opposed flow regime in microgravity to a higher velocity one.

In an earlier work, Bhattacharjee and Altenkirch (1990) investigated both the gas-phase and solid-phase radiation heat transfer effects on opposed flow spread over a thin solid fuel theoretically. Those investigators also predicted a radiation extinction limit, i.e. the same as that defined in Olson et al. (1988) and Olson (1991), in the low-velocity forced flow region. They concluded that the flame spread rate is higher when the fuel is subjected to the gas-phase radiation than when it is subjected to the solid-surface radiation only. Later, Bhattacharjee and Altenkirch (1991,1992) investigated how solid-surface radiation loss influences the thin fuel in a quiescent environment. According to their results, the rate of radiative heat losses from the flame and/or the surface increases with a lowering of the flow velocity, eventually leading to an extinction.

Duh and Chen (1993) included the surface radiative loss in their combustion model. Results obtained from their model indicated that both the flame strength and the spread rate decrease with a decrease of gravity level; an extinction limit was predicted as well. While considering both the gas-phase and surface radiative loss, Chen and Cheng (1994) described the gas-phase radiation by using a two-flux method in the cross-stream direction only. Numerical results revealed

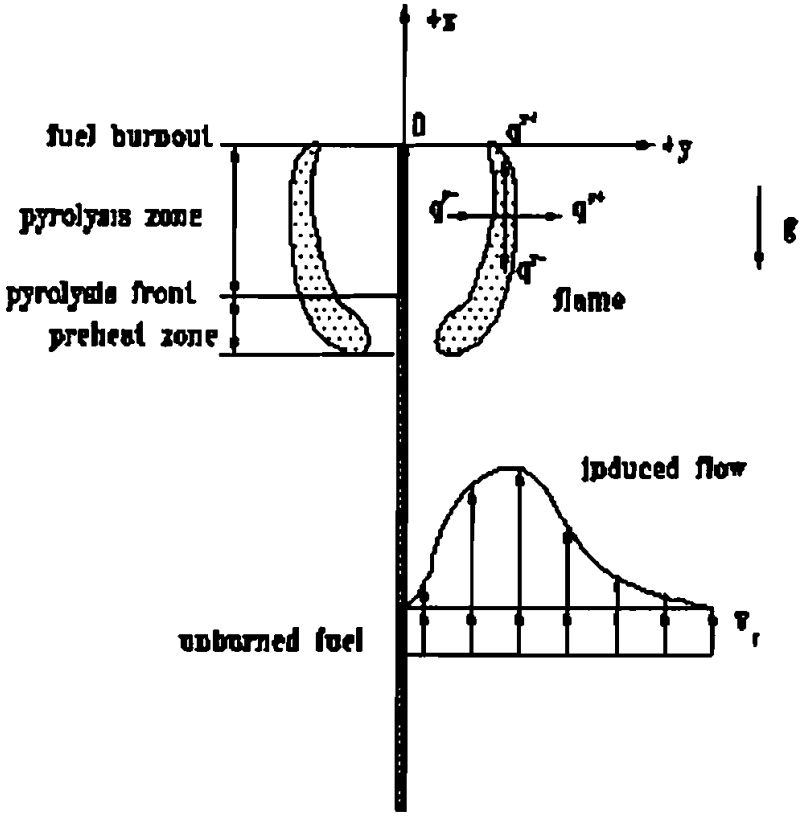

FIGURE 1 Schematic of flame over a thin fuel

that a quenching limit exists in the low gravity regime, which is inaccessible if radiation is neglected. Also this quenching limit can be sustained at a higher flame spread rate than that when merely considering surface radiative loss.

In light of above developments, this work not only investigates how radiation influences the flame spread behaviors, but also investigates how the stream-wise radiation affects the spreading flame by comparing with the corresponding flame structures obtained by the works of Duh and Chen (1991), Chen and Cheng (1994). To achieve those objectives, this work incorporates a radiation model including both the cross-stream and stream-wise gas-phase radiation coupled with solid-phase radiation with the combustion model of Duh and Chen (1991). The radiation model proposed herein allows us to identify the controlling mechanisms in different gravity regimes.

MATHEMATICAL MODEL

Figure 1 schematically depicts the configuration of downward flame spread over thin fuel. Both cross-stream and stream-wise gas radiation are simultaneously considered in the flame. For brevity, the development of mathematical model and it normalization procedure are omitted here. Details they can be found in Chen and Cheng (1994). Herein, we only describe the two-dimensional radiation model in detail, as given later. Table I summarizes the nondimensional gas phase governing equations. For momentum and species equations, their boundary conditions are a follows:

$$\text{at } x = x_{min} \quad u = V_f,\ v = 0,\ T = 1,\ Y_F = Y_C = Y_H = 0,\ Y_O^+ = 1 \tag{1}$$

$$\text{at } x = x_{max} \quad \frac{\partial u}{\partial x} = \frac{\partial v}{\partial x} = \frac{\partial T}{\partial x} = \frac{\partial Y_F}{\partial x} = \frac{\partial Y_O^+}{\partial x} = \frac{\partial Y_C}{\partial x} = \frac{\partial Y_H}{\partial x} = 0 \tag{2}$$

$$\text{at } y = 0, \text{ for } x_{min} < x < 0 \quad u = V_f,\ T_w = T_s,\ m_w'' = \rho_w v_w$$

$$\begin{aligned} m_w'' &= (\rho v Y_F)_w - \frac{\mu}{Pr \cdot \sqrt{Gr} \cdot Le} \cdot \left.\frac{\partial Y_F}{\partial y}\right|_w \\ m'' Y_{O,w}^+ &= \frac{\mu}{Pr \cdot \sqrt{Gr} \cdot Le} \cdot \left.\frac{\partial Y_O^+}{\partial y}\right|_w \quad , \quad i = C, H \\ m'' Y_{i,w} &= \frac{\mu}{Pr \cdot \sqrt{Gr} \cdot Le} \cdot \left.\frac{\partial Y_i}{\partial y}\right|_w \end{aligned} \tag{3}$$

$$\text{at } y = 0, \text{ for } 0 < x < x_{max} \quad \frac{\partial u}{\partial y} = v = 0 = \frac{\partial T}{\partial y} = \frac{\partial Y_F}{\partial y} = \frac{\partial Y_0^+}{\partial y} = \frac{\partial Y_C}{\partial y} = \frac{\partial Y_H}{\partial y} \tag{4}$$

$$\text{at } y = y_{max} \quad \frac{\partial u}{\partial y} = \frac{\partial v}{\partial y} = 0,\ T = 1,\ Y_F = Y_C = Y_H = 0,\ Y_O^+ = 1 \tag{5}$$

The radiation terms appearing in energy equation (Table I), q_x^r and q_y^r, are described by a two-dimensional P-1 approximation, which resembles that in Lauriat (1982). The P-N approximation assumes that the angular distribution of radiation intensity in a medium can be approximated by a finite series of spherical harmonics. By taking moments of the transfer equations and boundary conditions, all of the governing differential integral equations can be transformed into a set of partial differential equations. This approximation is appropriate for analyzing two and three dimensional problems. Examples can be found in Ratzel and Howell (1983) and Menguc and Viskanta (1984). Such an approximation does not require rotating this coordinates. Therefore, it is more feasible than that

of the four-flux approximation, in which the coordinates must be rotated 45°. By using P-1 approximation for the rectangular enclosure, the zeroth moment P.D.E. can be obtained in a dimensionless form as follows:

$$\frac{\partial^2 I_0}{\partial x^2}+\frac{\partial^2 I_0}{\partial y^2}=-3K_p^2\,(T^4-I_0) \tag{6}$$

where I_0 denotes the zeroth moment of radiation intensity, and K_p represents the dimensionless Planck mean absorption coefficient, which is discussed later. Equation (6) is subjected to the following boundary conditions:

1. at $x = x_{min}$

$$\left(1-\frac{2}{3K_p}\frac{\partial}{\partial x}\right) I_0 = 1$$

2. at $x = x_{max}$

$$\frac{\partial I_0}{\partial x} = 0$$

3. at $y = y_{max}$

$$\left(1-\frac{2}{3K_p}\frac{\partial}{\partial y}\right) I_0 = 1$$

4. at $y = 0$, $x_{min} \le x \le 0$

$$\frac{1}{\varepsilon}\left(1-\frac{2}{3K_p}\frac{\partial}{\partial y}\right) I_0 = T_s^4$$

5. at $y = 0$, $0 \le x \le x_{max}$

$$\frac{\partial I_0}{\partial y} = 0$$

Once the zeroth moment of radiation intensity, I_0, is obtained, then the gas phase radiation heat flux can be calculated from the following equations:

$$q_x^r = -\frac{1}{3K_p}\frac{\partial I_0}{\partial x} \tag{7}$$

$$q_y^r = -\frac{1}{3K_p}\frac{\partial I_0}{\partial y} \tag{8}$$

By using Eqs. (6), (7) and (8), the energy equation can be rewritten as

$$\rho u\frac{\partial T}{\partial x}+\rho v\frac{\partial T}{\partial y}=\frac{1}{Pr\cdot\sqrt{Gr}}\left[\frac{\partial}{\partial x}\left(\mu\frac{\partial T}{\partial x}\right)+\frac{\partial}{\partial y}\left(\mu\frac{\partial T}{\partial y}\right)\right]-q\dot{\omega}_F-\frac{K_p}{N_\infty}(T^4-I_0) \tag{9}$$

where $1/N_\infty$ is the radiation to conduction parameter and K_p denotes the Planck mean absorption coefficient. The definitions of N_∞ and K_p can be expressed as

$$N_\infty = \frac{\bar{k}^* \bar{v}_r}{\bar{\sigma} \cdot \bar{\alpha} \bar{T}_\infty^3} = \frac{\bar{k}^* \cdot (\bar{T}_\infty / \bar{\delta})}{\bar{\sigma} \cdot \bar{T}_\infty^4}$$

$$K_p = \bar{K}_p \cdot \bar{\delta} \tag{10}$$

where N_∞ represents a ratio of the conduction heat flux to radiation heat flux and K_p is a function of the temperature and composition of the mixture. The major contributors to thermal radiation are water vapor and carbon dioxide. Therefore, the general expression for the Planck mean coefficient K_p for the mixture can be written as

$$K_p = X(CO_2) \cdot K_p(CO_2) + X(H_2O) \cdot K_p(H_2O) \tag{11}$$

where X denotes the molar fraction. T'ien (1968) plotted the values of K_p for each species as a function of temperature. Notably, K_p decreases with an increase of temperature.

TABLE I Gas Phase Governing Equation

$$\frac{\partial}{\partial x}(\rho u \phi) + \frac{\partial}{\partial y}(\rho v \phi) = \left[\frac{\partial}{\partial x}\left(\Gamma \frac{\partial \phi}{\partial x}\right) + \frac{\partial}{\partial y}\left(\Gamma \frac{\partial \phi}{\partial y}\right)\right] + S$$

Equation	ϕ	Γ	S
Continuity	1		
x-Momentum	u	$\frac{\mu}{\sqrt{Gr}}$	$-\frac{\partial p}{\partial x} + S_u + \frac{\rho_\infty - \rho}{\rho_\infty - \rho_f}$
y-Momentum	v	$\frac{\mu}{\sqrt{Gr}}$	$-\frac{\partial p}{\partial y} + S_v$
Energy	T	$\frac{\mu}{Pr \cdot \sqrt{Gr}}$	$-q \cdot \dot{\omega}_F - \frac{1}{N_\infty}(\nabla \cdot q^r)$
Fuel	Y_F	$\frac{\mu}{Pr \cdot \sqrt{Gr} \cdot Le}$	$\dot{\omega}_F$
Oxidizer	Y_O^+	$\frac{\mu}{Pr \cdot \sqrt{Gr} \cdot Le}$	$f_O \cdot \dot{\omega}_F^+$
Carbon dioxide	Y_C	$\frac{\mu}{Pr \cdot \sqrt{Gr} \cdot Le}$	$-f_C \cdot \dot{\omega}_F$
Water vapor	Y_H	$\frac{\mu}{Pr \cdot \sqrt{Gr} \cdot Le}$	$-f_H \cdot \dot{\omega}_F$

where

$$S_u = \frac{1}{3}\frac{\partial}{\partial x}\left(\frac{\mu}{\sqrt{Gr}} \cdot \frac{\partial u}{\partial x}\right) + \frac{\partial}{\partial y}\left(\frac{\mu}{\sqrt{Gr}} \cdot \frac{\partial v}{\partial x}\right) - \frac{2}{3} \cdot \frac{\partial}{\partial x}\left(\frac{\mu}{\sqrt{Gr}} \cdot \frac{\partial v}{\partial y}\right)$$

$$S_v = \frac{1}{3}\frac{\partial}{\partial y}\left(\frac{\mu}{\sqrt{Gr}} \cdot \frac{\partial v}{\partial y}\right) + \frac{\partial}{\partial x}\left(\frac{\mu}{\sqrt{Gr}} \cdot \frac{\partial u}{\partial y}\right) - \frac{2}{3} \cdot \frac{\partial}{\partial y}\left(\frac{\mu}{\sqrt{Gr}} \cdot \frac{\partial u}{\partial x}\right)$$

$$\dot{\omega}_F = -Da \cdot \rho^2 Y_F Y_O^+ \exp(-E/T)$$

$$\dot{\omega}_F^+ = -Da^+ \cdot \rho^2 Y_F Y_O^+ \exp(-E/T)$$

The solid-phase governing equations for energy and mass conservation are as follows:

Energy balance equation:

$$\rho_s V_f \frac{dT_s}{dx} - \alpha_s \frac{d^2 T_s}{dx^2} = \frac{\mu}{\tau \, Pr \cdot \sqrt{Gr}} \cdot \left.\frac{\partial T}{\partial y}\right|_w + \frac{1}{\tau N_\infty}\left[\varepsilon\left(1 - T_s^4\right) + \frac{1}{3K_p} \cdot \left.\frac{\partial I_0}{\partial y}\right|_w\right]$$
$$+ m_s'' \cdot [L + (1 - c)(T_s - 1)] \tag{12}$$

The first two terms on RHS in the above equation represent the contributions from the surface conduction flux and the radiation flux, respectively.

Mass balance equation:

$$m_s'' = -V_f \frac{d\rho_s}{dx} = A_s \cdot \frac{\rho_s - \rho_{s,f}}{1 - \rho_{s,f}} \cdot \exp\left(-E_s/T_s\right) \tag{13}$$

According to the mass balance in Eq. (11), the flame spread rate is related to the integral of the nondimensional surface mass flux distribution as

$$V_f = \frac{1}{(1 - \rho_{s,f})} \cdot \int_{-\infty}^{0} m_s'' dx \tag{14}$$

The integral is numerically evaluated point by point via the distribution of mass flux.

Herein, the system of nonlinear, coupled partial differential equations is numerically solved. The model is approximated by an algebraic system using the finite difference scheme based on the SIMPLEC algorithm (Van Doormaal and Raithby, 1984). The computation was performed out on an SGI Indigo 2 workstation at National Chiao Tung University.

RESULTS AND DISCUSSION

The solid fuel is referred to as a paper towel, a monomer cellulose material, $C_6H_{10}O_5$. Table II lists all of the physical properties in gas and solid phase. These properties are basically the same as those used in Duh and Chen (1991) and Chen and Cheng (1994), allowing us to make a proper comparison later. The thermodynamic properties in the gas phase are evaluated at reference temperature $(\overline{T}^*)$. Table III lists the dimensionless parameters derived from the normalization procedure through the governing systems. Among these parameters, the most important ones are the Damkohler number (Da) and radiation to conduction

parameter ($1/N_\infty$), which was mentioned in energy equation, Eq. (9), and discussed later. The parametric study is based on the variation of gravity, which changes Da and $1/N_\infty$ simultaneously. Next, the computation is performed from the quenching limit (g=0.022) to the blowoff limit (g=4.5) under the specified ambient oxygen concentration, $Y_{O,\infty}$=0.233. Table IV lists the numerical results.

TABLE II Gas and Solid Property Values

Symbol	*Unit*	*Value*	*Reference*
$\overline{\rho}^*$	g/cm^3	f($Y_{O,\infty}$)	NBS (1955)
$\overline{k}^*$	W/cm·K	f($Y_{O,\infty}$)	NBS (1955)
$\overline{\mu}^*$	g/cm·sec	f($Y_{O,\infty}$)	NBS (1955)
$\overline{C}_p$	J/g·K	f($Y_{O,\infty}$)	NBS (1955)
$\overline{R}$	J/mole·k	8.314	NBS (1955)
$\overline{T}_v$	K	723	Hirano et. al. (1974)
$\overline{T}_\infty$	K	298	Duh and Chen (1991)
$\overline{r}$	cm	1.0×10^{-2}	Frey and T'ien (1977)
$\overline{T}_f$	K	f($Y_{O,\infty}$)	Altenkirch (1980)
$\overline{q}$	J/g	1.674×10^4	Altenkirch (1980)
$\overline{L}$	J/g	753	Altenkirch (1980)
$\overline{C}_s$	J/g·K	1.260	Altenkirch (1980)
$\overline{\rho}_{s,\infty}$	g/cm^3	0.650	Frey and T'ien (1977)
$Y_{O,\infty}$	-	0.233	Altenkirch (1980)
$\overline{E}$	J/mole	1.325×10^5	Chen (1990)
$\overline{B}$	cm^3/mole·sec	1.578×10^{12}	Chen (1990)
$\overline{k}_s$	W/cm·K	1.255×10^{-3}	Frey and T'ien (1977)
$\overline{E}_s$	J/mole	1.398×10^5	Lewellen et. al. (1977)
$\overline{A}_s$	1/sec	0.679×10^{10}	Lewellen et. al. (1977)
ε	-	0.92	Hirano et. al. (1974)

TABLE III Nondimensional Parameters

Symbol	*Parameter group*	*Value*
Pr	$\overline{\nu}/\overline{\alpha}$	0.702
Gr	$\overline{g}(\overline{\rho}_\infty - \overline{\rho}_f)\overline{\delta}^3/\overline{\rho}^*\overline{\nu}^{*2}$	2.028
Le	$\overline{\alpha}/\overline{D}$	1.000
Da	$Y_{O,\infty}\cdot\overline{B}\cdot\overline{\rho}^*\overline{\alpha}^*/\overline{V}_r^2$	variable
C	$\overline{C}_p/\overline{C}_s$	$f(Y_{O,\infty})$
γ	$\overline{T}^*/\overline{T}_\infty$	$f(Y_{O,\infty})$
T_v	$\overline{T}_v/\overline{T}_\infty$	2.426
E	$\overline{E}/\overline{RT}_\infty$	54.576
q	$\overline{q}/\overline{C}_p\overline{T}_\infty$	45.224
τ	$\overline{\tau}\overline{C}_s\overline{\rho}_s^*\overline{V}_r/\overline{k}^*$	variable
$\rho_{s,f}$	$\overline{\rho}_{s,f}/\overline{\rho}_s^*$	0.070
k_s	$\overline{k}_s/\overline{k}^*$	0.783
L	$\overline{L}/\overline{C}_s\overline{T}_\infty$	-2.012
A_s	$\overline{A}_s\overline{\alpha}^*/\overline{V}_r^2$	variable
E_s	$\overline{E}_s/\overline{RT}_\infty$	56.433
N_∞	$\overline{k}^*\overline{V}_r/\overline{\sigma}\overline{T}_\infty^3\overline{\alpha}^*$	variable

Figure 2 displays the flame spread rate $(\overline{V}_f)$ as a function of gravity level. To further understand how stream-wise radiation contributes to the spreading flame, three cases are presented: (a) no radiation, (b) 1-D gas-phase coupled with solid-phase radiation (Chen and Cheng, 1994), and (c) 2-D gas-phase with solid-phase radiation (present study).

For case (a), the results are exactly the same as those reported in Duh and Chen(1991). According to their investigation, the nondimensional flame spread rate (V_f), without considering the radiation effect, is proportional to Da, i.e., $\overline{V}_f \sim \overline{V}_r^{-1} \sim (\overline{g})^{-1/3}$. Increasing the strength of buoyant flow by increasing the gravity level reduces the penetration of forward heat conduction, subsequently

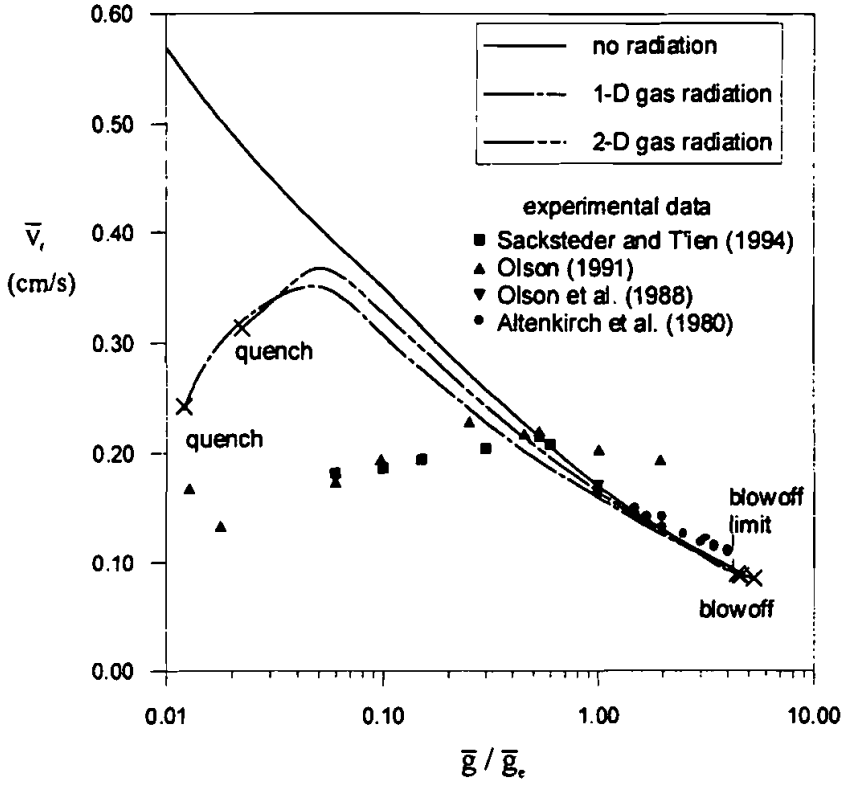

FIGURE 2 Flame spread rate ($\overline{V}_f$) versus gravity level (g)

producing a lower flame spread rate. As the limit, g=5.3, is reached, the flame blows off. This occurrence is commonly referred to as the flame stretch effect, which can be indicated by Da sole. However, the predicted behavior in the low-gravity regime, where the flame becomes stronger, contradicts what was observed in the drop-tower experiments. This contradiction is owing to that no other heat losses, e.g. radiation loss, are considered in that combustion model.

According to cases (b) and (c) in Fig. 2, incorporating radiation affects the profile of flame spread rate. It shows that the flame spread rate is lowered as the flame is subjected to radiation. However, the blowoff limits for both radiation cases become less (g = 4.3 for case (b) and g = 4.5 for case (c)). In the regime of $g \geq 0.04$ or 0.05, the radiation influence seems not too substantial. The trend of flame spread rate is still retained and increases with a decrease of gravity; however, the discrepancy from the one without radiation (case (a)) becomes greater and greater. This phenomenon indicates that forward heat transfer, or

Damkohler number (Da), still takes control on the flame behaviors; however, the radiation effect ($1/N_\infty$) gradually appears as the gravity level becomes lower. The maximal values of flame spread rate for cases (b) and (c) are 0.3578 cm/s at g = 0.04 and 0.3681 cm/s at g = 0.05, respectively. Thereafter, the flame spread rate for both cases starts to decrease rather than increase and dramatically decreases as the gravity is further reduced, indicating that the radiation influence becomes dominant. Finally, extinction occurs when each limiting gravity is reached.

TABLE IV Parametric Study (Effect of Changing Gravity Level)

g	$\overline{V}_f$ (cm/s)	$\overline{V}_r$ (cm/s)	$\overline{\delta}$ (cm)	$1/N_\infty$ (10^{-2})	Da (10^{10})
0.022	0.3129	7.094	0.4949	7.5472	2.5660
0.030	0.3360	7.867	0.4463	6.8120	2.0873
0.040	0.3604	8.659	0.4055	6.1805	1.7232
0.050	0.3681	9.327	0.3764	5.7405	1.4850
0.060	0.3676	9.912	0.3542	5.3996	1.3152
0.100	0.3259	11.751	0.2987	4.5600	0.9353
0.150	0.2966	13.452	0.2610	3.9793	0.7138
0.200	0.2729	14.806	0.2371	3.6206	0.5892
0.500	0.2068	20.095	0.1747	2.6603	0.3199
1.000	0.1621	25.318	0.1387	2.1101	0.2015
2.000	0.1282	31.899	0.1101	1.6801	0.1269
3.000	0.1089	36.515	0.0961	1.4699	0.0969
4.000	0.0934	40.190	0.0874	1.3300	0.0780
4.500	0.0814	41.800	0.0840	1.2799	0.0739

In the present model, two competing mechanisms exist for spreading flame which are forward heat conduction and radiation in gas phase, respectively. It can be referred to Eq. (9) as well. The gas phase radiation model is two-dimensional in this combustion model, and it has two kinds of contributions. One is to reduce the flame strength by losing heat to the ambient. The other one is that the heat loss from the flame joins the upstream conduction to reinforce the total forward heat transfer rate and the subsequent preheating of upstream virgin fuel to increase the flame spread rate. The latter effect, i.e. the stream-wise radiation heat transfer, could not be described in the model of Chen and Cheng (1994);

case (b). Figure 2 reveals that the flame spread rate in the present model (case (c)) is always lower than that in case (a). This finding suggests that the effect of losing heat from the flame caused by radiation apparently is greater than the one which contributes to the forward heat transfer. On the other hand, except for around g = 0.02, the flame spread rate in the present case is always greater than that in case (b), implying that the contribution of radiation in forward heat transfer shows up. The propagating flame in the present model can be survived up to g = 0.022, whereas it can be sustained further up to g = 0.012 in case (b). This finding indicates that heat loss due to radiation becomes dominant in the very low gravity (or microgravity) regime. Therefore, we can conclude that the radiation heat transfer significantly influences the microgravity combustion phenomena.

From a mathematical perspective, Eq. (9) reveals that the nondimensional energy equation consists of four terms: convection, conduction, heat generation and radiation, respectively. The heat generation is a source term, whereas the radiation is a heat loss one. Since the equation has been normalized, their relative orders of magnitude are determined by the corresponding parameters appearing just ahead of themselves. Physically, Damkohler number, Da, represents a ratio of flow residence time to chemical reaction time, and radiation to conduction parameter, K_p/N_∞, represents the ratio of radiation heat flux to conduction heat flux. As mentioned earlier, K_p itself, the nondimensional Planck mean absorption coefficient, is not prescribed in advance but provided as a part of solution. A representative profile will be given later in Fig. 7. According to this definition, Da is proportional to $(g)^{-2/3}$ and $1/N_\infty$ is $(g)^{-1/3}$, indicating that they are coupled together. By incorporating with Eq. (9), the larger the Da implies a stronger flame; its spread rate is expected to be faster. On the other hand, the larger the $1/N_\infty$ implies that the flame loses more heat to ambient and becomes weaker; however, it implicitly leads to a stronger forward heat transfer, as mentioned earlier. Table IV lists the values of Da and $1/N_\infty$ as a function of gravity.

At a higher gravity level, such as $g \geq 2$, although Da heavily influences the flame structure, the influence of $1/N_\infty$ is only slight, as confirmed by Fig. 2 where the three profiles are nearly coincident. As the gravity level becomes lower, Da is increased, indicating that the flame becomes stronger. However, $1/N_\infty$ is also increased , thereby intensifying the radiation heat loss. These two competing effects result in a lower flame spread rate, but still with an ascending trend. Up to a certain gravity, such as g = 0.05 in the present model is reached, the effect of $1/N_\infty$ completely outweighs that of Da. Thereafter, the flame spread rate decreases with a decrement of gravity. Finally, the flame can no longer survive in an extremely low gravity level, such as $g < 0.022$ in the present model.

To illustrate the radiation influence in a low gravity environment, Fig. 3 plots three flame structures selected at g = 0.03, near the extinction limit in the present

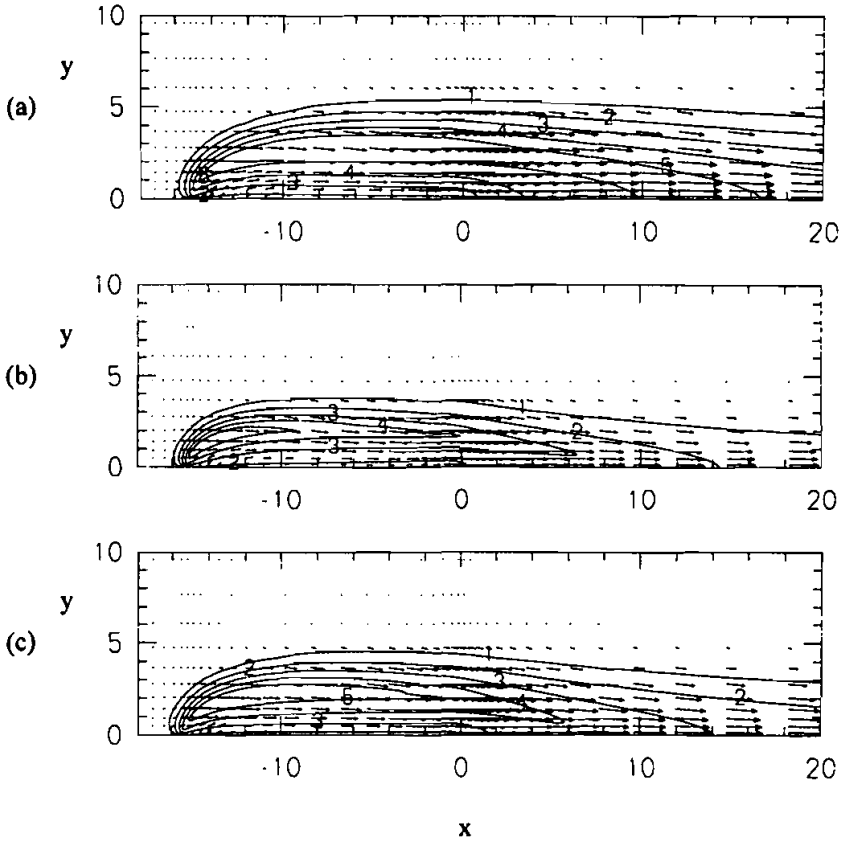

FIGURE 3 Isotherm and velocity distributions (g=0.03, $Y_{O,\infty}$ =0.233) (a) No radiation. (b) One-dimensional model radiation. (c) Tow-dimensional model radiation

case, which is a combination of gas phase isotherms and velocity vector distributions. Herein, we designate the area enclosed by isotherm T=5 (or 1200°C dimensionally) as the flame zone, similar to the flame appearance of the Schlieren photographs taken by Duh (1992). For case (a), the flame has the largest flame size and highest flame temperature among the three cases. This finding suggests that it is the strongest flame. This is expected because no heat loss is considered in this case. The flame zone in case (b) is the smallest and the flame temperature is the lowest. This event implies that the radiation effect contributes primarily to heat loss; there is no contribution to forward heat transfer at all. The following discussion confirms this assumption. Also, according to our results, the flame zone encloses the burnout point completely whereas the flame zones in the radiation cases only exist on the side of fuel plate. This phenomenon, i.e. the

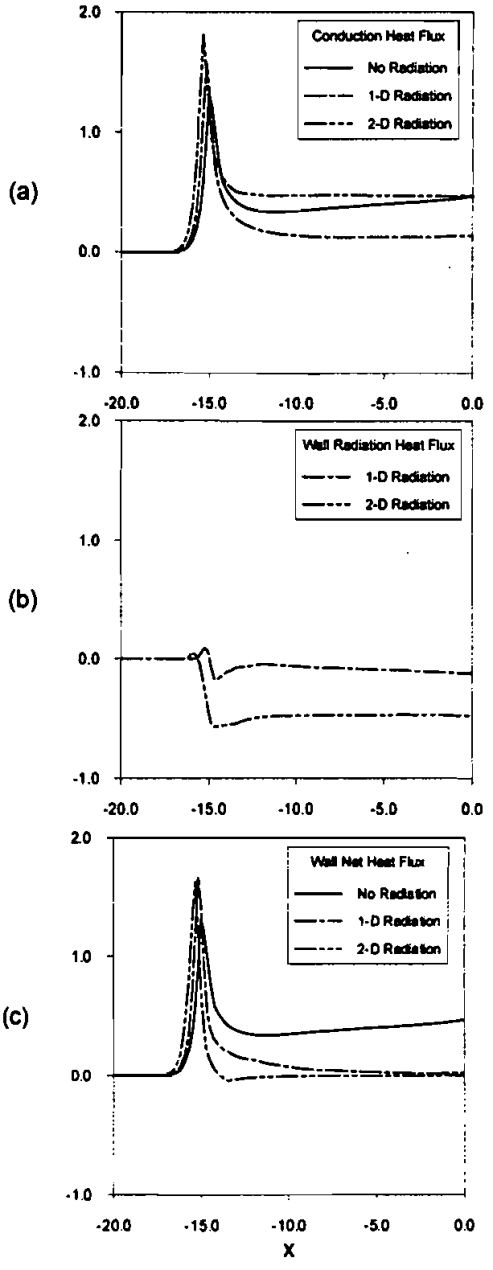

FIGURE 4 Heat flux distributions (g=0.03, $Y_{O,\infty}$=0.233), (a) Conduction heat flux distribution. (b) Radiation heat flux distribution. (c) Net wall heat flux

flame tail is open and does not enclose the burnout point, was observed in microgravity experiments by Vedha-Nayagan and Altenkirch (1986) and Olson (1988), respectively.

The flame in case (c) is stronger and has a larger flame size than that in case (b). Also, the flame front of case (c) appears to extend the furthest upstream among these three spreading flames, as confirmed in Figs. 5 and 6. From above discussion, we can infer that gas radiation in the stream-wise direction can transfer heat efficiently to both upstream and downstream directions in addition to the cross-stream direction. Consequently, it enhances the forward preheat effect, thereby increasing the strength of flame. Similarly, stream-wise radiation can further extend the combustion and thermal plumes in the downstream. However, the contribution to forward heat transfer apparently is less than that of heat loss to ambient. Therefore, the strength of flame in case (c) decays more dramatically and reaches a quenching limit more quickly as gravity is further lowered.

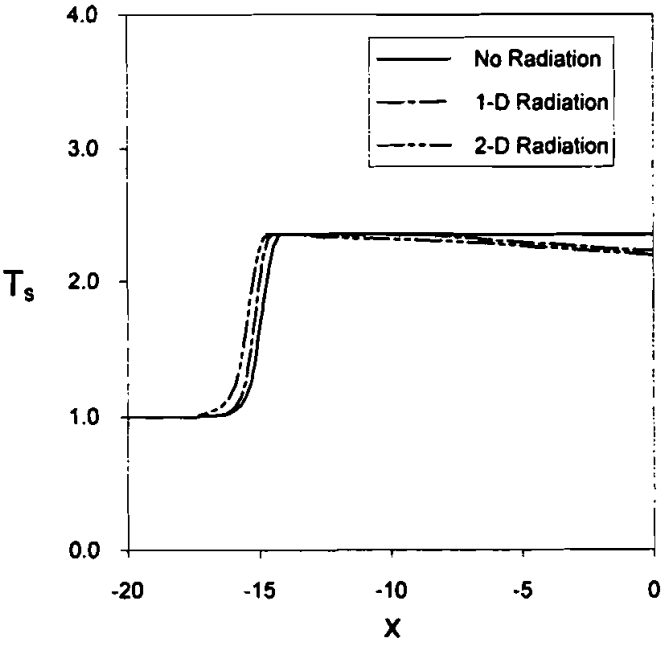

FIGURE 5 Solid fuel temperature distributions. (g=0.03, $Y_{O,\infty}$=0.233)

Figure 4 shows the wall heat flux distributions for the conduction, the net radiation, and the summation of the last two in low gravity (g=0.03). In Fig. 4(a), no radiation case has the maximal conduction and total heat flux due to the strongest flame structure. The 2-D radiation model has a larger conduction heat transfer

into wall than the 1-D radiation model since its flame zone is larger and closer to the surface. According to Fig. 4(b), 2-D radiation model has a greater amount of net radiative heat loss in the pyrolysis zone, initiated from $x = -15$ to burnout point $x = 0$. It implies that the radiative heat loss from surface is much greater than that gained from the flame. This is despite the fact that case (b) has a similar trend but not so severe. Fig. 4 (c) displays the total heat flux distributions for these three flames. Interestingly, for both radiative cases, the portions behind the spikes are nearly flat, particularly for the 2-D model with a value of approximately zero. These distributions markedly differ from those for the case without radiative effect. Figure 3 also confirms that the flame zone ($T = 5$) ceases ahead of burnout point in the radiation cases. Bhattacharjee and Altenkirch (1991) observed this phenomenon, for the first time, in drop-tower experiment. Actually, a similar prediction appeared in an earlier work (Bhattacharjee and Altenkirch, 1991), while applying a simple gas-radiation approximation to a spreading flame model.

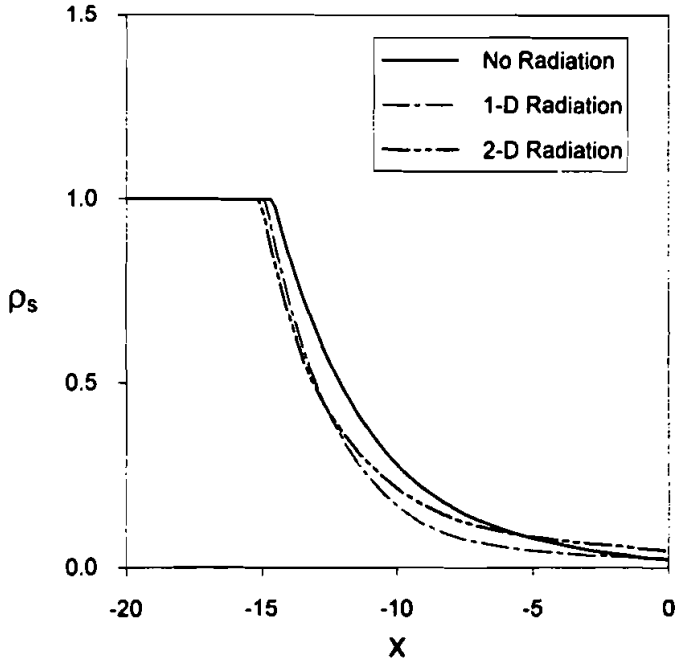

FIGURE 6 Solid fuel density distributions. ($g=0.03$, $Y_{O,\infty}=0.233$)

Figure 5 depicts the surface temperature distribution along the fuel surface for these three cases. As mentioned earlier, the burnout point is located at $x = 0$ and the pyrolysis front commences from the position, where local solid density,

ρ_s, = 0.99, as shown in Fig. 6. According to this figure, the preheating of upstream virgin fuel occurs earlier for both radiation cases. As expected, it occurs furthest upstream for case (c). In the pyrolysis region, the surface temperature for no-radiation case is maintained constant along with the pyrolysis temperature. For the other two cases, the constant surface temperature region only exits around the flame front area and, then, gradually decreases towards the burnout point. This finding suggests that the surface radiation loss becomes significant in the downstream of flame front since the flame is shifted away from the surface, as indicated in Fig. 3. The present model has the lowest values in surface temperature and constant surface temperature area because it is subjected to the lowest total heat flux.

Figure 6 depicts the solid fuel density distributions. These three curves monotonically decreases from pyrolysis front to burnout point. Radiation does not appear to markedly affect the profiles since the solid density is sole determined by surface temperature. However, the solid density for the present model starts to become greater than the one in case (b) around x = −13. This tendency is owing to that the surface temperature in former case is lower than the one in the latter case. As mentioned earlier in the previous figures, the pyrolysis front for the present case is located furthest upstream due to the stream-wise radiation effect. It also indicates that the corresponding flame has the longest pyrolysis length.

Figure 7 shows the distribution of nondimensional Planck mean coefficient (K_p) for g = 0.03. This figure serves as an indicator of the gas phase radiation source distribution. Recall that K_p is not prescribed, but provided as a part of solution since it is a function of the temperature and the concentrations of combustion products, such as carbon dioxide (CO_2) and water vapor (H_2O); see Eq. (11). However, as mentioned earlier, the dimensional value of $\overline{K}_p$ for each species decreases with an increase of temperature (Tien, 1968). According to this figure, the value of $K_p$outside the flame is quite small since the concentrations of CO_2 and H_2O are of trace amount in the ambient. Near the fuel plate, the amount of CO_2 and H_2O are somewhat significant and the temperature is not too high. Therefore, the highest K_p occurs over there. Chen and Chang (1996) observed the same behavior. That study numerically investigated the counterflow diffusion flame subjected to the gas-phase radiation. In the thermal plume in far downstream of burnout point, there exists a significant K_p zone (=0.014). This zone is because both the CO_2 and H_2O are convected from upstream reaction zone to downstream and the local temperature is lowered due to the mixing with ambient cold air. This contributes to elongate the thermal plume, consequently, it is longer than the one in Fig. 3(b). Finally, the maximal dimensional value of $\overline{K}_p$ (corresponding to K_p = 0.026) is 0.058 1/cm, thereby ensuring that the requirement for the optically-thin assumption holds.

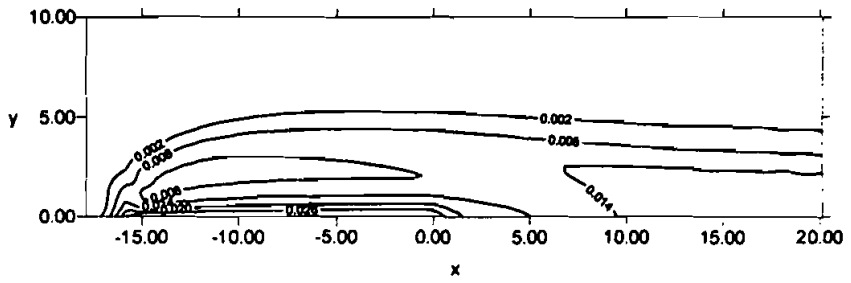

FIGURE 7 Nondimensional Planck mean absorption coefficient distribution. (g=0.03, $Y_{O,\infty}$=0.233)

As mentioned earlier, many important features of 2-D radiation model have been pointed out. The radiation model used in this work is a four-flux model, which considers radiative heat transfer in both cross-stream and stream-wise direction. In a real situation, radiation is a multi-dimensional phenomenon. The stream-wise radiation transfers extra energy from the flame to join in the forward heat conduction to increase the flame spread rate. Meanwhile, the drawing out of energy by radiation reduces the flame itself strength, resulting in a slower spreading flame. Exactly how these two competing mechanisms interact with each other and, then, determine the flame behavior has already been discussed. Finally, the pioneering work of Bhattacharjee and Altenkirch (1990) is worth mentioning, which applied an emission model to describe the gas phase radiation heat transfer. The radiation term appeared in energy equation is $4a_p\ \sigma(T^4-T_\infty^4)$, which is a phenomenological approach. It treats the flame as a gas layer without including the radiation contribution from the solid surface. Also, the formula for obtaining a_p may be inappropriate because it is a function of local temperature but not of ambient temperature. Although these shortcomings might lead to incorrect quantitative results, this study predicts (for the first time) the qualitative trend in microgravity spreading flame.

Comparisons with Experiments

Figure 2 summarizes some of the available experimental data as well. Such data are adopted from Altenkirch et. al., (1980), Olson et al. (1988), Olson (1991), and Sacksteder and T'ien (1994). The fact that the solid fuel thickness and density used in the natural-covective experiments are differ from those used herein accounts for why the measured flame spread rates are modified by their respective area densities to compare with the ones predicted herein. Olson et. al. (1988) and Olson (1991) adopted the same treatment because, for a thin fuel, de Ris

(1969) contended that the flame spread rate varies inversely with area density. For comparison with flame spread results under the forced convection environment, Olson (1991) suggested that the characteristic velocities used in forced convection experiments correspond to the ones obtained from natural convection environments using a buoyant velocity, $V_b = (\alpha\ g(T_f-T_\infty)/T_\infty)^{1/3}$ to deduce the specific gravity level, corresponding to that of forced flow velocity.

Comparing prediction and measurement results reveals that the qualitative trends in flame spread rate for both cases correlate with each other. Restated, in addition to having the non-monotonic trend of flame spread with the gravity level, both cases have a high gravity blowoff limit as well as a quench limit in low gravity. In the elevated gravity regime, g>1.0, the predicted spread rates correlate well with the experimental data of Altenkirch et. al. (1980); the critical gravities of blowoff limits are extremely close to each other as well. At normal gravity, the predicted results confer with the measurement results of Olson et al. (1988) and Altenkirch et al. (1980). For the partial-gravity experimental data of Sacksteder and T'ien (1994), although the flame spread rate at g=0.6 closely resembles our prediction, the discrepancy becomes increasingly greater as the gravity is lowered. For the data converted from the forced flow experiments in air (Olson, 1991), two of the experiment closely approach the present values at g = 0.25 and 0.45; the other values in lower gravity levels are deviated significantly. The latter behavior can be found in higher gravity levels as well, which is also observed in the comparison with Olson (1991) in flame spread by Sacksteder and T'ien (1994). Exactly why prediction results deviate from experimental ones, particularly in a low gravity regime, is explained later. The flammability boundary drawn in Sacksteder and T'ien (1994) reveals that a quench limit should exist between 0.05g and zero-g in 21% oxygen environment. Our computational results predict that the flame is to be extinguished at 0.022g, which is within that domain. However, as g≤0.2, the predicted values markedly deviate from the experimental data, which is similar to the comparison with Olson (1991) as mentioned earlier. For example, the computed peak flame spread rate occurs at g=0.05, whereas the peak is experimentally found at g=0.6 in Sacksteder and T'ien (1994). This finding suggests that the radiation effect on flame spread rate in this model is under-predicted in an extremely low gravity regime.

Although the source of discrepancy in a low-gravity environment is unclear, it is believed that P-1 approximation incorporated in this combustion model may be inaccurate at a relatively low optical thickness. The applicability of P-1 approximation is constrained by the temperature, optical thickness and boundary conditions; it is particularly appropriate for an optical dense medium (Ratzel and Howell, 1983). Thus, it may not reflect an actual situation under normal experimental conditions and the assumptions in this study. Moreover, using the

Planck-mean absorption coefficient without modification may over-predict the radiation emission and under-predict self-absorption (T'ien and Bedir, 1997). Another contributing factor could be the selection of kinetics and radiation parameters. Therefore, a sensitivity study in these parameters should be undertaken to evaluate the ability of the present flame spread model to quantitatively predict the low gravity regime more accurately.

CONCLUSIONS

This investigation numerically studies a flame spread over a thermally-thin solid fuel under the influence of two-dimensional gas radiation over a wide range of gravity level. Via normalization procedure, the two most important parameters, Damkohler number, Da, and radiation to conduction parameter, $1/N_\infty$, are identified, respectively. Mathematically, Da is proportional to $(g)^{-2/3}$ and $1/N_\infty$ is $(g)^{-1/3}$, indicating that both interact with each other. The computational domain ranges from the quenching limit $(0.022\overline{g}_e)$ in a low gravity regime to the blow-off limit $(4.5\overline{g}_e)$ in high gravity. The computed results are from two previous studies, Duh and Chen (1991); no radiation case, and Chen and Cheng (1994); with cross-stream radiation only, are also included in the presentation to identify how the radiation affects the spreading flame and, subsequently, differentiates the stream wise radiation contribution from this effect through the relative comparisons. In a high gravity regime, Da is predominant and $1/N_\infty$ is minor, indicating that flame stretch is the dominant mechanism for spreading flame and radiation is not as important. As the gravity is lowered, the flame spread rate still maintains the trend of increasing with a decrease of gravity; however, its value is less than that without considering the radiation effect. This finding implies that influence of radiation gradually appears. As gravity reaches $0.05\overline{g}_e$, radiation effect completely takes control because the flame spread decreases rather than increases with a decrease of gravity. It quickly approached extinction as the gravity is further reduced. Except for the flame spread rate as a function of gravity, the flame structures in gas phase and the heat flux, temperature and density distributions along the solid fuel at a specified gravity, $g = 0.03$, are plotted graphically as well to illustrate the difference among these three flames. Regarding stream wise radiation, it consists of two competing factors. One is to draw energy out from the flame to reduce the flame strength. Then, this heat loss via radiation can reinforces the forward heat transfer ahead of flame front to increase the flame spread rate. As expected, the flame temperature is lowered in radiation cases. On the other hand, the flame front extends furthest upstream in the present case. In addition, it has a longer combustion and thermal plumes in downstream

comparing to the one obtained from Chen and Cheng (1994). However, the former effect surpasses the latter one since the flame spread rate in the present model is always lower than that predicted by Duh and Chen (1991). Finally, the contour of Planck mean absorption coefficient in gas phase demonstrates the gas phase radiation distribution. The most significant radiation occurs near the pyrolysis surface and the other one is in the downstream of burnout point.

NOMENCLATURE

A_S	Pre-exponential factor for fuel pyrolysis, $\bar{A}_s\bar{\alpha}^*/\bar{V}_r\bar{V}_f$
$\bar{B}$	Pre-exponential factor for gas-phase reaction
C	Ratio of specific heat, $\bar{C}_p/\bar{C}_s$
$\bar{C}_p$	Specific heat for gas mixture
$\bar{C}_s$	Specific heat for solid fuel
$\bar{D}$	Species diffusivity
Da^+	Modified Damkohler number, $\bar{B}\bar{\rho}^*\bar{\delta}/\bar{V}_r$
Da	Damkohler number, $Y_{O,\infty}\cdot Da^+$
E	Activation energy, $\bar{E}/\bar{R}\bar{T}_\infty$
f_c	Stoichiometric CO_2/fuel mass ratio
f_H	Stoichiometric H_2O/fuel mass ratio
f_o	Stoichiometric oxidizer/fuel mass ratio
g	Gravitational acceleration, $\bar{g}/\bar{g}_e$
$\bar{g}_e$	Normal earth gravity
Gr	Grashof number, $\bar{g}(\bar{\rho}_\infty-\bar{\rho}_f)\bar{\delta}^3/\bar{\rho}^*\bar{\nu}^{*2}$
$\bar{I}_0$	Zeroth moment of intensity
$\bar{k}$	Conductivity
$\bar{k}_p$	Planck mean absorption coefficient
L	Latent heat, $\bar{L}/\bar{C}_s\bar{T}_\infty$
Le	Lewis number
$\bar{m}''$	Surface pyrolysis mass flux rate

N_∞	The conduction-radiation parameter based on $\overline{T}_\infty$
P	Pressure, $(\overline{p}-\overline{p}_\infty)/\overline{\rho}^*\overline{V}_r^2$
Pr	Prandtl number, $\overline{\nu}/\overline{\alpha}$
$\overline{q}$	Heat of combustion per unit mass of fuel
$\overline{R}$	Universal gas constant
T	Temperature, $\overline{T}/\overline{T_\infty}$
$\overline{T_v}$	Vaporization temperature
u	Velocity parallel to the fuel surface, $\overline{u}/\overline{V_r}$
v	Velocity normal to the fuel surface, $\overline{v}/\overline{V_r}$
V_f	Nondimensional flame spread rate, $\overline{V}_f/\overline{V}_r$
$\overline{V_r}$	Reference velocity, $[\overline{g}(\overline{\rho}_\infty-\overline{\rho}_f)\overline{\alpha}^*/\overline{\rho}^*]^{1/3}$
x	Distance parallel to the fuel surface, $\overline{x}/\overline{\delta}$
x_{max}	Location of downstream boundary
x_{min}	Location of upstream boundary
y	Distance normal to the fuel surface, $\overline{y}/\overline{\delta}$
Y	Concentration
Y_O^+	The normalized oxygen concentration, $Y_O/Y_{O,\infty}$
y_{max}	Location of boundary far from the wall
γ	Temperature ratio, $\overline{T}^*/\overline{T_\infty}$
$\overline{\alpha}$	Thermal diffusivity
ε	Emissivity
$\overline{\delta}$	Thermal length, $\overline{\alpha}^*/\overline{V_r}$
μ	Dynamic viscosity, $\overline{\mu}/\overline{\mu}^*$
$\overline{\nu}$	Kinematic viscosity
ρ	Density of gas phase, $\overline{\rho}/\overline{\rho}^*$
ρ_s	Density of solid phase, $\overline{\rho}_s/\overline{\rho}_{s\infty}$
$\dot{\omega}$	Reaction rate, $-Da\cdot\rho^2 Y_F Y_O \exp(-E/T)$
τ	Fuel-bed half thickness, $\overline{\tau}\overline{C}_s\overline{\rho}_{s\infty}\overline{V}_f/\overline{k}^*$
Overhead	

-	Dimensional quantities
Superscripts	
*	Reference state on $\bar{T}$
"	Flux
Subscripts	
f	Flame
F	Gaseous fuel
O	Oxidizer
S	Solid phase
W	Fuel wall
∞	Ambient conditions

Acknowledgements

The authors would like to thank the National Science Council of the Republic of China for financially supporting this research under Contract No. NSC86–2612-E009–004

References

Altenkirch, R. A., Eichhorn, R., and Shang, P. C. (1980). Buoyancy Effects on Flame Spreading down Thermally Thin Fuel, *Combustion and Flame* **37**, 71–83.

Bhattacharjee, S., Altenkrich, R. A., Olson, S. L. and Sotos, R. G. (1988). Heat Transfer to a Thin Solid Combustible in Flame Spreading at Microgravity, *Eastern section/* The Combustion Institute.

Bhattacharjee, S., Altenkirch, R. A., (1990). Radiation-Controlled, Opposed-Flow Flame Spread in a Microgravity Environment, *23rd Symposium (International) on Combustion,* The Combustion Institute. 1627–1633.

Bhattacharjee, S., Altenkirch, R. A., (1991). The Effect of Surface Radiation on Flame Spread in a Quiescent. Microgravity Environment, *Combustion and Flame,* **84,** 160–169.

Bhattacharjee, S., Altenkirch, R. A., and Sacksteder, k., Implications of spread rate and temperature of flame spread on a thin fuel in quiescent, Microgravity, space base environment, *Combustion Science and Technology,* **91,** 225–242.

Chen, C. H. (1990). A Numerical Study of Flame Spread and Blowoff Over Thermally Thin Solid Fuel in an Opposed Air Flow, *Combustion Science and Technology,* **69,** 63–83.

Chen, C. H. and Cheng, M. C. (1994). Gas Phase Radiative Effects on downward Flame Spread in Low Gravity, *Combustion Science and Technology,* **97,** 63–83.

Chen, C. H. and Chang, K. H. (1996). Counterflow Diffusion Flame with Gas-Phase Radiation, *Journal of the Chinese Society of Mechanical Engineers,* **17,** 1,81–92.

DeRis. J. N. (1969). Spread of a Laminar Diffusion Flame. *Twelfth Symposium (International) on Combustion.* The Combustion Institute. 241.

Duh, F. C. and Chen, C. H. (1991). A Theory for Downward Flame Spread Over a Thermal-thin Fuel, *Combustion Science and Technology,* **77,** 291–305.

Duh, F. C. and Chen, C. H. (1993). Flame Spread Over a Thermally-thin Solid Fuel in Zero Gravity, *Warme-und Stoffubertagung,* **28,** 81–88.

Duh, F. C. (1992). Theoretical and Experimental Analyses of Downward Flame Spread Over a Thermally Thin Fuel, Ph.D. Dissertation, National Chiao-Tung University, HsinChu, Taiwan.

Fakheri, A. and Olson, S. L. (1989). The Effects of Radiative Hear Loss on Microgravity Flame Spread, *AIAA paper* 89–0504.

Frey, A. E. and T'ien, J. S. (1977). A Theory of Flame Spread Over a Solid Fuel Including Finite-Rate Chemical Kinetics, Rep. FTAS/TR-77–134, Case Western Reserve University, Cleveland, OH. 82.

Lauriat, G. (1982). Combined Radiation-Convection in Gray Fluids Enclosed in Vertical Cavities, *Journal of Heat Transfer,* **104,** 609–615.

Menguc, M. C. and Viskanta, R. (1984). Radiative Transfer in Three-Dimensional Rectangular Enclosures Containing Inhomogeneous, Anisotropically Scattering Media, *Journal Quantitative spectroscopy radiation transfer* **33,** 533–549.

Olson, S. L. (1987). The Effect of Microgravity on Flame Spread Over a Thin Fuel, *MS Thesis,* Case Western Reserve University, Cleveland.

Olson, S. L., Ferkul, P. V. and T'ien, J. S. (1988). Near-limit Flame Spread Over a Thin Solid Fuel in Microgravity, *22nd Symposium (international) on Combustion,* The Combustion Institute, Pittsburgh, 1213–1222.

Olson, S. L., (1991) Mechanisms of Microgravity Flame Spread Over a Thin Solid Fuel: Oxygen and Opposed Flow Effects. *Combustion Science and Technology,* 76, 233–249.

Patankar, S. V. (1980). *Numerical Heat Transfer and Fluid Flow,* McGraw Hill, New York.

Ratzel III, A. C. and Howell, J. R. (1983). Two-Dimensional Relation in Absorbing-Emitting Media Using The P-N Approximation, *Journal of Heat Transfer,* **105,** 333–340.

Sacksteder, K. R. and T'ien, J. S. (1994), Buoyant Downward Diffusion Flame Spread and Extinction in Partial-Gravity Accelerations, *25th Symposium (International) on Combustion,* 1685–1692.

T'ien, J. S. and Bedir, H., Radiative Extinction of Diffusion Flames – A Review, *Asia-Pacific Conference on Combustion,* Osaka, Japan, May 1997.

T'ien, C. L. (1968). *Thermal Radiation Properties of Gases-Advances in Heat Transfer,* Academic Press, New York 5, 254–234.

Van Doormaal. J. P. and Raithby, G. D. (1984). Enhancements of the SIMPLE Methods for Predicting incompressible Fluid Flow. *Numerical Heat Transfer* **7,** 147–163.

Vedha-Nayagam, M. and Altenkirch, R. A. (1986). The Shape of Low-Gravity Flame Spreading Across Combustible Surface, *Central States Section,* The Combustion Institute.